Floquet topological phases and skin effects in periodically driven non-Hermitian systems

Kaiye Shi [1,2,3] Liwei Qiao [2,3] Zhiyue Zheng, [1,*] and Wei Zhang [2,3,1,†]
[1] *Beijing Academy of Quantum Information Sciences, Beijing 100193, China*
[2] *Department of Physics and Beijing Key Laboratory of Opto-electronic Functional Materials and Micro-nano Devices, Renmin University of China, Beijing 100872, China*
[3] *Key Laboratory of Quantum State Construction and Manipulation (Ministry of Education), Renmin University of China, Beijing 100872, China*

(Received 7 April 2024; revised 8 July 2024; accepted 12 August 2024; published 26 August 2024)

We study a non-Hermitian Su-Schrieffer-Heeger model with nonreciprocal hopping under periodic driving, and show that the Floquet topological nature and non-Hermiticity can have rich interplay in this non-Hermitian Floquet topological system. We find that both the topological characteristics and the non-Hermitian skin effect are affected by the Floquet driving and can be associated with the quasienergy spectrum topology. For general choice of system and driving parameters, we derive a non-Bloch bulk-boundary correspondence to successfully describe the Floquet topological edge states with non-Hermitian skin effects. We observe interesting bipolar non-Hermitian skin effect by periodically driving the short-range non-Hermitian system, and establish its connection to the winding of Bloch quasienergy spectrum. Finally, we propose to implement the non-Hermitian quantum system with asymmetric hopping in cold atomic gases. Our work demonstrates the impact of periodic driving on non-Hermitian topological systems, and suggests a route to search for richer non-Hermitian skin effects through Floquet engineering.

DOI: 10.1103/PhysRevA.110.022222

I. INTRODUCTION

In the framework of standard quantum mechanics, the Hamiltonian describing a closed system is considered to be Hermitian. However, most physical systems under realistic conditions are inevitably exchanging energy or constituent with environment and cannot be considered as strictly closed. When the coupling with the environment is prominent, as in various classical [1–3] and quantum [4–6] systems with notable dissipation, and in phenomenological models of quasiparticles with a finite lifetime [7,8], an effective non-Hermitian Hamiltonian can be formulated to describe the steady state and dynamics upon nonunitary evolution [9–11]. Recently, topological phenomena of non-Hermitian systems have attracted extensive attention from both the theoretical [12–25] and experimental aspects [26–32]. The interplay between non-Hermiticity and topology can lead to a failure of the bulk-boundary correspondence (BBC) well established for Hermitian systems [12,14–16,18,20,33–35], bring in richer topological classification [36–38], stabilize exotic topological phases without Hermitian counterparts [39–42], and result in many other novel phenomena [43–48]. In particular, the conventional BBC must be replaced by a modified version known as non-Bloch BBC [14,15], which is established based on non-Bloch topological invariants defined in the generalized Brillouin zone (GBZ) [15,18,49,50]. The breakdown of conventional BBC is attributed to the non-Hermitian skin effect (NHSE) [15,33,51,52] with all bulk eigenstates accumulating to boundaries of the system, which is related to the nontrivial winding of Bloch spectrum on the complex plane [53]. When long-range hopping is introduced, the Bloch spectrum will undergo a twist, making the bulk eigenstates accumulate in different directions. This phenomenon is known as bipolar NHSE, which has received widespread attention [34,54,55]. Further consideration of interactions within a unit cell may even lead to many-body bipolar NHSE [56]. In addition, the nontrivial interplay between NHSE and topological modes can lead to the occurrence of a hybrid skin-topological effect in high-dimensional systems [25,57], where topological angular modes can be generated without higher-order topological origin.

Meanwhile, coherent control via periodic driving can also enrich the scope of topological states. Under the so-called Floquet engineering technique [58–60], the conventional static phases can be driven into various types of Floquet topological phases [61–65]. In the past decade, much attention has been paid to Hermitian systems under Floquet driving, which leads to the discovery of richer phase diagrams with many exotic topological phases [66–72]. Most of such phases cannot be characterized by the conventional topological invariants used in their corresponding static models. For example, the topological properties of a static noninteracting two-dimensional lattice model without additional symmetry are fully described by the Chern number [73]. However, Chern number is not sufficient to determine the chirality and number of quasienergy edge modes of such model under periodic driving. Owing to the existence of π modes in Floquet quasienergy spectrum, a so-called anomalous Floquet topological phase is found with

*Contact author: zhengzy@baqis.ac.cn
†Contact author: wzhangl@ruc.edu.cn

robust topological edge modes but zero Chern numbers for all bands [74,75]. The anomalous Floquet topological system has been realized in photonic crystals [64,65] and ultracold atomic gases [76,77]. Recently, Floquet engineering has been introduced to non-Hermitian systems to assist the exploration of more exotic phases [78–84]. Studies suggest that in some special circumstances; e.g., when certain characteristic polynomials can be truncated at lower orders [82,83] or when the GBZ is a circle [84], the non-Hermitian BBC can be safely applied to Floquet cases. However, a discussion of non-Hermitian Floquet topological phases under general conditions is still lacking.

In this work, we consider a periodically driving non-Hermitian Su-Schrieffer-Heeger (SSH) model and investigate the effect of Floquet engineering on topological properties and NHSE. Owing to the complex form of the effective Floquet Hamiltonian, an analytical solution of the associated GBZ does not exist in general. Instead, we rely on numerical methods to solve for the Floquet GBZ without truncating the effective Hamiltonian [82,83] and demonstrate the non-Hermitian Floquet BBC. More interestingly, we demonstrate that the introduction of the temporal dimension provides a way to regulate the effective Floquet GBZ, which in turn affects the NHSE. Specifically, we observe an interesting bipolar NHSE where skin modes are present on both boundaries of the system and are connected by the complex winding of Bloch bulk spectrum. With the knowledge of GBZ for general cases, we can establish a correspondence between the spatial distribution of skin modes and the winding of loops in bulk spectrum. Furthermore, we find that the Floquet bands without NHSE can be realized, even when the instantaneous Hamiltonian is always nonreciprocal. The non-Hermitian Floquet SSH model and the novel bipolar NHSE can be demonstrated using cold atoms trapped in a state-dependent one-dimensional optical lattice.

The remainder of the paper is organized as follows. In Sec. II we introduce the non-Hermitian SSH model under periodic driving. In Sec. III we discuss two typical driving schemes and calculate their corresponding Floquet GBZ to accurately capture the topological characteristics. In Sec. IV we provide an intuitive picture to understand how Floquet engineering affects GBZ and NHSE. The relation between non-Hermitian skin modes and the winding of a Bloch spectrum is discussed. Finally, we summarize and suggest an experimental proposal to implement the non-Hermitian Floquet SSH model with ultracold atoms in Sec. V.

II. NON-HERMITIAN SSH MODEL UNDER PERIODIC DRIVING

We consider a non-Hermitian SSH model with asymmetric intra-unit-cell hopping [15,85], as depicted in Fig. 1(a). The real-space Hamiltonian of a system with L unit cells reads

$$H=\sum_{j=1}^{L}[t_2(a_{j+1}^\dagger b_j+\text{H.c.})+(t_1+\gamma)a_j^\dagger b_j+(t_1-\gamma)b_j^\dagger a_j], \tag{1}$$

where a_i (b_i) is the annihilation operator of sublattice A (B) of the ith unit cell, and t_1 (t_2) is the average hopping integral within a unit cell (between neighboring cells). The non-Hermiticity is induced by the imbalance γ of the asymmetric intra-unit-cell hopping. The Hamiltonian satisfies a sublattice symmetry (also known as chiral symmetry [15,18]) $CHC^{-1}=-H$, with $C=\sigma_z\bigotimes\mathbb{I}_L$ and $\mathbb{I}_L$ the $L\times L$ identity matrix acting on all lattice cells. The symmetry ensures that the energy spectrum is symmetric about the origin. After Fourier transformation, the k-space Hamiltonian can be written as

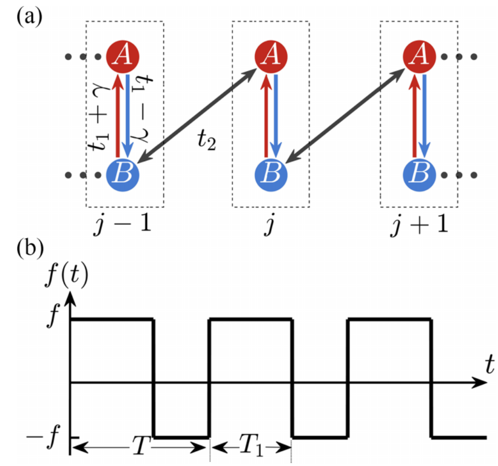

FIG. 1. (a) The non-Hermitian SSH model with nonreciprocal intracell hoppings $t_1+\gamma$ and $t_1-\gamma$, and intercell hopping t_2. (b) The scheme of periodic driving. The Hamiltonian parameters denoted by f change periodically over time in a two-stage square form.

$$\mathcal{H}(k)=(t_1+t_2\cos k)\sigma_x+(t_2\sin k+i\gamma)\sigma_y, \tag{2}$$

where σ's are Pauli operators acting on the pseudospin space $\{a,b\}$ formed by the two sublattices. The k-space Hamiltonian also acquires chiral symmetry $\mathcal{C}^{-1}\mathcal{H}(k)\mathcal{C}=-\mathcal{H}(k)$ with $\mathcal{C}=\sigma_z$, and the eigenvalues are $E_\pm(k)=\pm\sqrt{(t_1+t_2\cos k)^2+(t_2\sin k+i\gamma)^2}$. Apparently, most of the eigenvalues are complex regardless of the choice of parameters.

On the other hand, we can easily find that the energy spectrum of the real-space Hamiltonian Eq. (1) is real when $|\gamma|<|t_1|$. In fact, for the non-Hermitian model (1), we can apply a unitary transformation $U=(i\sigma_x+\mathbb{I}_2)/\sqrt{2}\bigotimes\mathbb{I}_L$ with $\mathbb{I}_2$ the 2×2 identity matrix acting on the two sublattices, and rewrite the real-space Hamiltonian into a form with parity-time-reversal ($\mathcal{PT}$) symmetry $H_{\mathcal{PT}}=U^{-1}HU$ [86]. The Hamiltonian $H_{\mathcal{PT}}$ has been studied in Ref. [12], and the condition $|\gamma|<|t_1|$ corresponds to the $\mathcal{PT}$-symmetry preserved phase where all eigenvalues are real (see the Appendix A). This observation shows that the energy spectrum of the Hamiltonian in real space and that in Bloch space are of stark difference, manifesting the phenomena of NHSE and the failure of conventional BBC.

One can rely on a suitable similarity transformation $\bar{H}=S^{-1}HS$ to restore BBC [15]. The similarity transformation is a diagonal matrix $S=\text{diag}(1,r,r,\ldots,r^{L-1},r^L)$ for $|t_1|>|\gamma|$, where $r=\sqrt{|\frac{t_1-\gamma}{t_1+\gamma}|}$. The Bloch Hamiltonian after the transformation reads

$$\bar{\mathcal{H}}(k) = (\bar{t}_1 + \bar{t}_2 \cos k)\sigma_x + \bar{t}_2 \sin k\sigma_y, \tag{3}$$

where $\bar{t}_1 = \sqrt{t_1^2 - \gamma^2}$ and $\bar{t}_2 = t_2$. The transformed real-space Hamiltonian $\bar{H}$ and its Bloch form $\bar{\mathcal{H}}(k)$ correspond to a standard Hermitian SSH model and belong to the BDI (AIII) class for real (complex) hopping in the Altland-Zirnbauer classification [87,88]. The topology of the BDI (AIII) class is characterized by a $\mathbb{Z}$ invariant [89], known as the winding number

$$w = \frac{1}{4\pi i} \int_{1\mathrm{BZ}} \mathrm{Tr}[\mathcal{C}QdQ], \tag{4}$$

where $Q(k) = |\phi_+(k)\rangle\langle\phi_+(k)| - |\phi_-(k)\rangle\langle\phi_-(k)|$, $|\phi_\pm(k)\rangle$ are eigenstates of the Bloch Hamiltonian, and the integration is restricted within the first Brillouin zone (1BZ).

The method outlined above is also applicable in the $\mathcal{PT}$-symmetry broken regime $|\gamma| > |t_1|$. At this time, we should choose the similarity transformation as $\bar{S} = \mathrm{diag}(1, \bar{r}, \bar{r}, \ldots, \bar{r}^{L-1}, \bar{r}^L)$ with $\bar{r} = \sqrt{\frac{t_1-\gamma}{t_1+\gamma}}$. The Bloch Hamiltonian is identical to Eq. (3), but with a complex $\bar{t}_1$ and hence is non-Hermitian. The topological invariant of the non-Hermitian Hamiltonian can still be chosen as the winding number defined in Eq. (4), which can effectively capture the information of edge states. Notice that since the Hamiltonian is non-Hermitian, $Q(k)$ should be changed to $Q(k) = |\phi_r(k)\rangle\langle\phi_l(k)| - |\bar{\phi}_r(k)\rangle\langle\bar{\phi}_l(k)|$, where $|\phi_{r/l}(k)\rangle$ and $|\bar{\phi}_{r/l}(k)\rangle$ are chiral-symmetric eigenstates of the Bloch Hamiltonian, and $|\phi_l(k)\rangle$ satisfies $\bar{\mathcal{H}}^\dagger(k)|\phi_l(k)\rangle = E^*(k)|\phi_l(k)\rangle$. This observation shows that non-Hermiticity does not necessarily lead to the failure of BBC.

On the basis of the static non-Hermitian SSH model (1), next we consider a periodic variation of parameters such that the Hamiltonian becomes periodic in time, i.e., $H(t + T) = H(t)$ with period T. The periodically time-dependent Hamiltonian extends the energy of an equilibrium state to quasienergy ε of a dynamically steady state, which characterizes the irreducible representation of the time-shifted symmetry group. The discrete time translational symmetry makes quasienergy a periodic variable defined in the first Floquet Brillouin zone $[-\pi/T, \pi/T)$, similar to the quasimomentum of a lattice with discrete space translational symmetry. The topological characterization of Floquet systems are defined upon the quasienergy spectrum, whose nontrivial winding may lead to the existence of topological protected edge states. The Floquet quasienergy bands can be inscribed using an effective Floquet Hamiltonian $H_{\mathrm{eff}} = i \ln U_T/T$, where the Floquet operator $U_T = \mathbb{T} e^{\int_0^T -iH(t)dt}$ is a one-period evolution operator and $\mathbb{T}$ is time-ordering operator.

For the sake of definiteness and simplicity, in the following discussion we consider a two-stage driving protocol as illustrated in Fig. 1(b),

$$f(t) = \begin{cases} f, & [mT, mT + T_1), \\ -f, & [mT + T_1, (m+1)T), \end{cases} \quad m \in \mathbb{N}, \tag{5}$$

where $f(t)$ is a short-hand notation of all time-dependent parameters. The instantaneous Hamiltonian corresponding to the first stage of $f(t) = f$ is denoted by H_1, while the second by H_2. Thus, the Floquet operator is simplified to $U_T = e^{-iH_2T_2}e^{-iH_1T_1}$. With the aid of the effective Hamiltonian H_{eff}, we can characterize the quasienergy spectrum of the Floquet system.

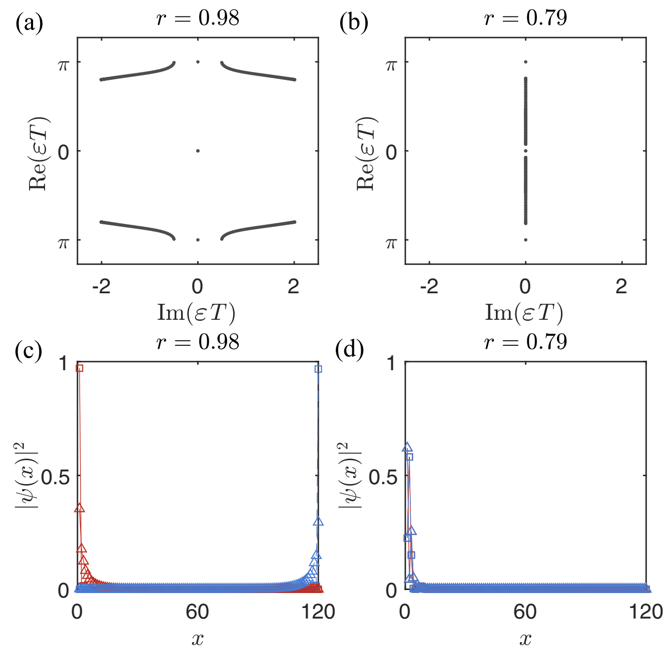

FIG. 2. The quasienergy spectrum of the effective Hamiltonian H_{eff} under open boundary condition (OBC) for a system of size $L = 120$, with (a) $t_1 = 0.005$ and (b) $t_1 = 1.4$. The intercell hopping t_2 is periodically riven between ± 1. In both cases, topological edge states are present with spatial distribution depicted respectively in (c) and (d). For (a) and (c), $|\gamma| > |t_1|$ and the system is in the $\mathcal{PT}$-symmetry broken region, where the edge modes are distributed on both edges. The case of (b) and (d), however, corresponds to the $\mathcal{PT}$-symmetry preserved region with $|\gamma| < |t_1|$ and edge state found at one edge only. Other parameters used are $\gamma = 0.32$, $T_1{:}T_2 = 4{:}1$, and $T = 2\pi$. In this plot and the ones following, we set the absolute value of t_2 as the energy unit, ε is the quasienergy, T is the driving period, and x represents the lattice cell index.

One simple example is to vary the inter-unit-cell hopping integral $t_2(t)$ between two opposite values t_2 and $-t_2$. As will be discussed in the next section, this choice of varying the parameter does not change the $\mathcal{PT}$ phase transition point or the GBZ. As shown in Figs. 2(a) and 2(b), there are both 0 modes and π modes in the quasienergy spectrum, which is a unique feature of Floquet systems. When $|\gamma| > |t_1|$ ($|\gamma| < |t_1|$), the non-Hermitian Floquet bands are complex (real), correspond to the $\mathcal{PT}$-symmetry broken (preserved) region as depicted in Fig. 2(a) [Fig. 2(b)].

Since the non-Hermitian skin modes are also distributed at the system boundaries, the difference between topological edge modes and skin modes is hardly distinguished from spatial distribution only. Nonetheless, since the topological edge modes are always fixed at the center of band gaps with quasienergy 0 or π/T, they are more stable in comparison to the non-Hermitian bulk modes accumulated at boundaries, especially in the $\mathcal{PT}$-symmetry broken region where the quasienergy spectrum is complex. In addition, the topological edge states can also be affected by the NHSE. When the parameter r approaches 1 as shown in Fig. 2(c), the NHSE is weak and the topological edge states can be found at both ends of the system but with asymmetric distributions. When r moves away from 1, the NHSE tends to restore by pushing all topological edge states towards one end of the system, as demonstrated in Fig. 2(d). The characterization of these topological edge modes and the interplay between NHSE and Floquet engineering are the central topics of this work.

III. NON-HERMITIAN FLOQUET BULK-BOUNDARY CORRESPONDENCE

In a Hermitian system, the bulk states are approximately the same under either open boundary condition (OBC) or periodic boundary condition (PBC), such that the topological invariants of the Bloch bands (obtained under PBC) correspond to the number of edge modes (present under OBC). In a non-Hermitian system with NHSE, however, the bulk characteristics of an OBC Hamiltonian cannot be approximated by the Bloch Hamiltonian under PBC. In order to obtain the correct BBC, a non-Bloch theory based on GBZ is used in static non-Hermitian system [14,15,18,49]. The same idea has also been tested for periodically driven systems in some special circumstances [82,84].

In this section we derive the BBC holds for more general non-Hermitian Floquet systems. We start from a brief review of the non-Bloch BBC for static one-dimensional Hamiltonian with chiral symmetry $\mathcal{C}$. By using β to replace e^{ik} of a Hamiltonian $\mathcal{H}(k)$ in Bloch space, we obtain the GBZ Hamiltonian $\mathcal{H}(\beta)$ satisfying the eigenvalue equation

$$\det[\mathcal{H}(\beta) - E] = 0. \tag{6}$$

The equation is an algebraic equation of even degree $2M$ about β and has $2M$ solutions. By arranging these solutions in order as $|\beta_1| \leqslant |\beta_2| \leqslant \cdots \leqslant |\beta_{2M-1}| \leqslant |\beta_{2M}|$, the GBZ C_β is the trajectory on which β_M and β_{M+1} satisfy [18]

$$|\beta_M| = |\beta_{M+1}|. \tag{7}$$

Then one can define the non-Bloch winding number in a similar mathematical expression as the Bloch winding number [15]

$$\tilde{w} = \frac{1}{4\pi i}\int_{\mathrm{GBZ}} \mathrm{Tr}\big[\mathcal{C}\tilde{Q}d\tilde{Q}\big], \tag{8}$$

where $\tilde{Q}(\beta) = |\phi_r(\beta)\rangle\langle\phi_l(\beta)| - |\bar{\phi}_r(\beta)\rangle\langle\bar{\phi}_l(\beta)|$, $|\phi_{r/l}(\beta)\rangle$ and $|\bar{\phi}_{r/l}(\beta)\rangle$ are chiral-symmetric eigenstates of the GBZ Hamiltonian, and $|\phi_l(\beta)\rangle$ satisfies $\mathcal{H}^\dagger(\beta)|\phi_l(\beta)\rangle = E^*(\beta)|\phi_l(\beta)\rangle$. When there is no NHSE in the system, the GBZ is a unit circle and the non-Bloch winding number (8) reduces to the Bloch one (4). In the presence of NHSE, the GBZ is deformed from the unit circle and the topological edge states are induced by the nontrivial topology of wave functions of $\mathcal{H}(\beta)$.

It is worth noting that the non-Bloch winding number can also be obtained in an intuitive way. Because the GBZ Hamiltonian has chiral symmetry $\mathcal{C}^{-1}\mathcal{H}(\beta)\mathcal{C} = -\mathcal{H}(\beta)$, we can represent $\mathcal{H}(\beta)$ as

$$\mathcal{H}(\beta) = \begin{pmatrix} 0 & R_+(\beta) \\ R_-(\beta) & 0 \end{pmatrix}. \tag{9}$$

Furthermore, the non-Bloch winding number can be expressed as [18]

$$\tilde{w} = -(1/4\pi)[\arg R_+(\beta) - \arg R_-(\beta)]_{C_\beta}. \tag{10}$$

That is, we can easily determine the non-Bloch winding number by the trajectories of the off-diagonal elements $R_\pm$. The continuous bands obtained from C_β and the ones obtained under OBC are consistent except for the edge state [18].

Now we turn to the discussion on periodically driven non-Hermitian systems. Periodic driving extends the topological classification from group $\mathcal{G}$ to group $\mathcal{G}^n$, where $\mathcal{G} = \{\emptyset, \mathbb{Z}, 2\mathbb{Z}, \mathbb{Z}_2, \mathbb{Z}\oplus\mathbb{Z}, 2\mathbb{Z}\oplus 2\mathbb{Z}, \mathbb{Z}_2\oplus\mathbb{Z}_2\}$ [38] and n is the number of gaps in the quasienergy spectrum that need to be considered. For the SSH model Eq. (1) with chiral symmetry, the topological class thus becomes $\mathbb{Z}\times\mathbb{Z}$ when subjected to a two-stage driving scheme, and is characterized by two topological invariants $\tilde{w}_0$ and $\tilde{w}_\pi$ associated with the 0 and π modes, respectively. To derive the topological invariants, we follow the same treatment as for Hermitian systems [68] and define two similar transformations $F_1(k) = e^{i\mathcal{H}_1(k)T_1/2}$ and $F_2(k) = e^{-i\mathcal{H}_2(k)T_2/2}$ associated with the two instantaneous Hamiltonians. From those, two new evolution operators can be obtained:

$$U'(k) = F_1^{-1}U_T(k)F_1, \quad U''(k) = F_2^{-1}U_T(k)F_2. \tag{11}$$

The corresponding effective Hamiltonians $\mathcal{H}'_{\mathrm{eff}}(k)$ and $\mathcal{H}''_{\mathrm{eff}}(k)$ have chiral symmetry $\mathcal{C}^{-1}\mathcal{H}(k)\mathcal{C} = -\mathcal{H}(k)$. Then we use β to replace e^{ik} to get GBZ Hamiltonians $\mathcal{H}'_{\mathrm{eff}}(\beta)$ and $\mathcal{H}''_{\mathrm{eff}}(\beta)$, and define the corresponding non-Bloch winding number $\tilde{w}'$ and $\tilde{w}''$ according to Eq. (8). Finally, we reach the topological invariants for the 0 and π modes of the Floquet system

$$\tilde{w}_0 = \frac{\tilde{w}' + \tilde{w}''}{2}, \quad \tilde{w}_\pi = \frac{\tilde{w}' - \tilde{w}''}{2}. \tag{12}$$

This definition of topological invariants can be understood as a natural generalization from Hermitian Floquet systems by using GBZ instead of the Brillouin zone. However, the calculation of such invariants can be technically challenging, since the expression of GBZ Hamiltonian $\mathcal{H}_{\mathrm{eff}}(\beta)$ in the Floquet system is in general very complicated. For the simple step-function driving scheme (5), an expression can be available but still does not have the simple polynomial form as in a static system. For other driving schemes, such as cosine functions, it is not even possible to write a clear expression for the effective Hamiltonian. Thus, the major difficulty in restoring BBC for non-Hermitian Floquet systems lies in the calculation of effective Floquet GBZ $C_\beta^{\mathrm{Floquet}}$ associated with the effective GBZ Hamiltonian $\mathcal{H}_{\mathrm{eff}}(\beta)$. To our knowledge, the non-Hermitian Floquet BBC is currently tested only when truncating the effective Hamiltonian [82,83] or when the generalized Brillouin zone is already known [84].

A. Periodically driving does not change the GBZ

We first consider the similar driving scheme as in Ref. [84], where the parameter under variation is $f(t) = t_2(t)$:

$$t_2(t) = \begin{cases} t_2, & [mT, mT + T_1), \\ -t_2, & [mT + T_1, (m+1)T), \end{cases} \quad m \in \mathbb{N}. \tag{13}$$

To calculate the non-Bloch winding numbers $\tilde{w}'$ and $\tilde{w}''$ according to Eq. (8), and subsequently the topological invariants $\tilde{w}_0$ and $\tilde{w}_\pi$, one needs to employ Eqs. (6) and (7) to calculate the Floquet GBZ C_β^{Floquet} of the effective generalized Hamiltonians $\mathcal{H}'_{\text{eff}}(\beta)$ and $\mathcal{H}''_{\text{eff}}(\beta)$. However, since the GBZ of $H(t)$ is a circle with radius $r = \sqrt{|\frac{t_1-\gamma}{t_1+\gamma}|}$, which is independent of the parameter $t_2(t)$, the Floquet GBZ under driving remains a circle with radius $r_F = r$. Thus, one can directly assume $\beta = re^{ik}$ and obtain the non-Hermitian BBC for this special occasion [84].

It is worth noting that for this particular driving scheme, we can remove NHSE through a similarity transformation $\bar{S}$ as for a static non-Hermitian system [15], and capture the topological characteristics using Bloch winding numbers, which can avoid the complicated calculation of Floquet GBZ. The instantaneous real-space Hamiltonians H_1 and H_2 can be transformed under the same similarity transformation $\bar{S} = \text{diag}(1, \bar{r}, \bar{r}, \dots, \bar{r}^{L-1}, \bar{r}^L)$ with $\bar{r} = \sqrt{\frac{t_1-\gamma}{t_1+\gamma}}$, leading to $\bar{H}_1$ and $\bar{H}_2$, respectively. The quasienergy spectrum of the effective Hamiltonian $\bar{H}_{\text{eff}}$ is identical to the original system. We then define two new evolution operators

$$\bar{U}' = \bar{F}_1^{-1}\bar{U}_T\bar{F}_1, \quad \bar{U}'' = \bar{F}_2^{-1}\bar{U}_T\bar{F}_2, \tag{14}$$

with the aid of invertible evolution operators $\bar{F}_1 = e^{i\bar{H}_1T_1/2}$ and $\bar{F}_2 = e^{-i\bar{H}_2T_2/2}$. Apparently, $\bar{U}'$ and $\bar{U}''$ describe evolutions starting at different times. The corresponding effective Hamiltonians $\bar{H}'_{\text{eff}}$ and $\bar{H}''_{\text{eff}}$ have chiral symmetry, and thus can be topologically characterized by integer winding numbers w' and w'', respectively. The bulk topological invariants w_0 and w_π of $\bar{H}_{\text{eff}}$ are obtained as in Eq. (12) and hold a direct correspondence to the number of 0 modes and π modes for H_{eff} as shown in Fig. 3.

B. Periodically driving changes the GBZ

Now we consider the driving protocol where both the inter-unit-cell hopping rate t_2 and non-Hermitian parameter γ oscillate over time:

$$[t_2(t), \gamma(t)] = \begin{cases} [t_2, \gamma], & [mT, mT + T_1), \\ [-t_2, -\gamma], & [mT + T_1, (m+1)T), \end{cases} \quad m \in \mathbb{N}. \tag{15}$$

In this scheme, the GBZs of $\mathcal{H}_1$ and $\mathcal{H}_2$ are circles with radii $r_1 = \sqrt{|\frac{t_1-\gamma}{t_1+\gamma}|}$ and $r_2 = \sqrt{|\frac{t_1+\gamma}{t_1-\gamma}|}$, respectively. The coupling between them hence can make the Floquet GBZ of the effective Hamiltonian $\mathcal{H}_{\text{eff}}$ an irregular closed curve. Owing to the complexity of the effective Hamiltonian, it is difficult to solve for GBZ semianalytically using Eqs. (6) and (7). One therefore has to rely on a numerical approach by replacing the eigenvalues of GBZ Hamiltonian with the eigenvalues of OBC

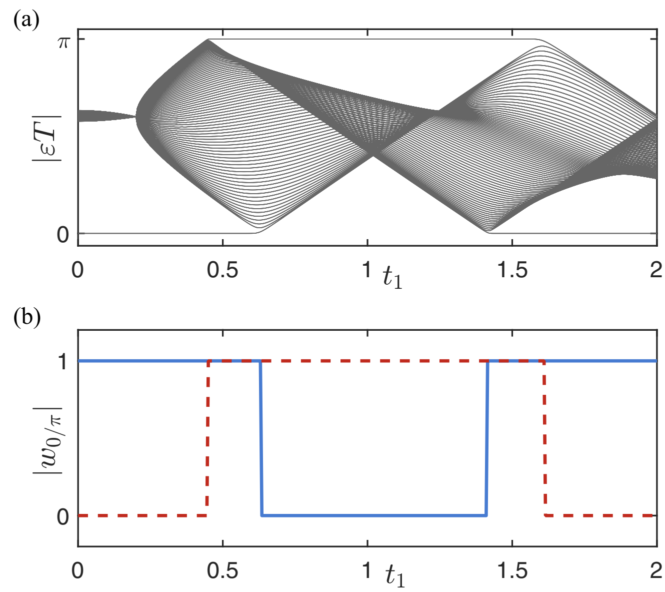

FIG. 3. (a) The quasienergy spectrum of the effective Hamiltonian under OBC for a system of size $L = 120$, with different choice of t_1 and oscillating $t_2 = \pm 1$. (b) The Bloch winding numbers $|w_{0/\pi}|$ as functions of t_1. The red solid line and blue dashed line represent $|w_\pi|$ and $|w_0|$, respectively. Other parameters used are $\gamma = 0.2$, T_1:T_2 = 4:1, and $T = \pi$.

Hamiltonian [15]. The essence behind this method is to make the bulk bands of OBC coincide well with those of the GBZ Hamiltonian $\mathcal{H}(\beta)$, such that the BBC can be restored. Despite its conceptual clarity, the numerical approach can be very costly in computational power, since the eigenvalues obtained by diagonalizing non-Hermitian Hamiltonian are sensitive to system size and spatial resolution [50].

In Fig. 4 we show some numerical results for a typical choice of driving parameters. As depicted in Fig. 4(a), the quasienergy spectra under OBC (gray solid line and gray dots) and PBC (blue dotted line) are significantly different. The Floquet Hamiltonian $\mathcal{H}_{\text{eff}}(\beta)$ is then assumed to have the same quasienergy spectrum as the OBC case, and the effective Floquet GBZ can be numerically obtained by solving Eq. (6), as shown in Fig. 4(b). Notably, the GBZ is deformed from a unit circle (dashed) and has an irregular shape with some part inside and some part outside the unit circle. The topological invariant $\tilde{w}'$ ($\tilde{w}''$) of the GBZ Hamiltonian $\mathcal{H}'_{\text{eff}}$ ($\mathcal{H}''_{\text{eff}}$) is calculated from the off-diagonal elements $R'_\pm$ ($R''_\pm$) defined in Eq. (9). From the results displayed in Figs. 4(c) and 4(d), we get $\tilde{w}' = +1$ and $\tilde{w}'' = -1$, and consequently $\tilde{w}_0 = 0$ and $\tilde{w}_\pi = +1$. These numbers predict the existence of a pair of topological π modes, inconsistent with the OBC spectrum given in Fig. 4(a) (gray dots).

Of particular interest is the special case of $T_1 = T/2$, where the net accumulation of hopping over the whole cycle is reciprocal, although both H_1 and H_2 are nonreciprocal. Under this condition, the bulk energy spectrum of a system under OBC [Fig. 5(a)] match perfectly that under PBC [Fig. 5(b)], and a pair of topological edge states are stably present at the zero energy gap and distributed on the sample edges [Fig. 5(c)]. The effective Floquet Hamiltonian does not present NHSE

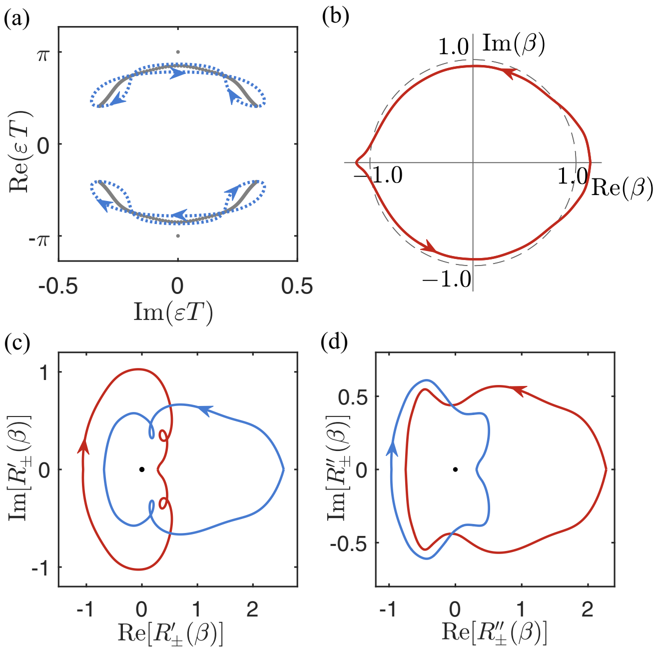

FIG. 4. Topological characterization of non-Hermitian Floquet topological phases by driving $t_2 = \pm 1$ and $\gamma = \pm 0.2$. (a) Quasienergy spectrum under OBC (gray solid line and gray dots) and PBC (blue dotted line). (b) The trajectory of Floquet GBZ in a complex plane (red solid line) deforms from the unit circle (gray dashed line). Panels (c) and (d) show the trajectories of $R'_\pm$ and $R''_\pm$, respectively. The system size is $L = 120$, and other parameters used are $t_1 = 0.95$, $T_1{:}T_2 = 3{:}2$, and $T = \pi$.

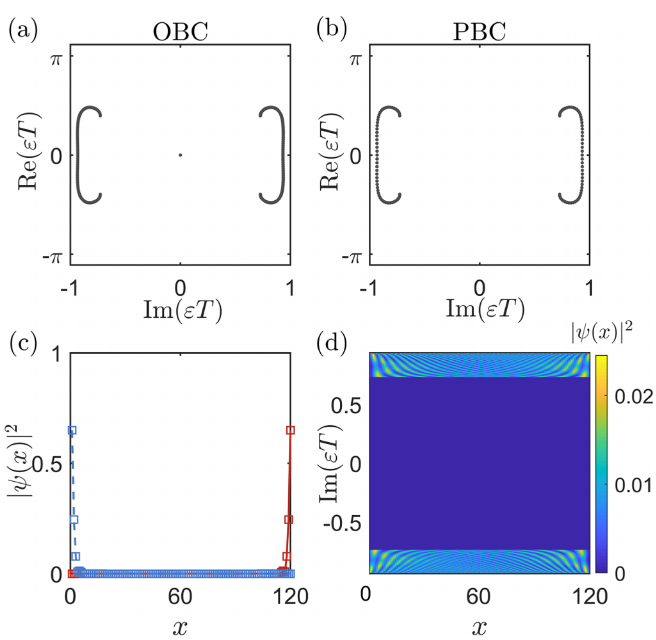

FIG. 5. (a) The quasienergy spectrum of the effective Hamiltonian under OBC for a system of size $L = 120$ with driving parameters $t_2 = \pm 1$ and $\gamma = \pm 0.4$. (b) The quasienergy spectrum of the effective Hamiltonian under PBC. (c) Distribution of topological edge modes in real space. (d) Modulus square (false color) of bulk modes in real space. Other parameters used are $t_1 = 1.3$, $T_1{:}T_2 = 1{:}1$, and $T = 1.5\pi$.

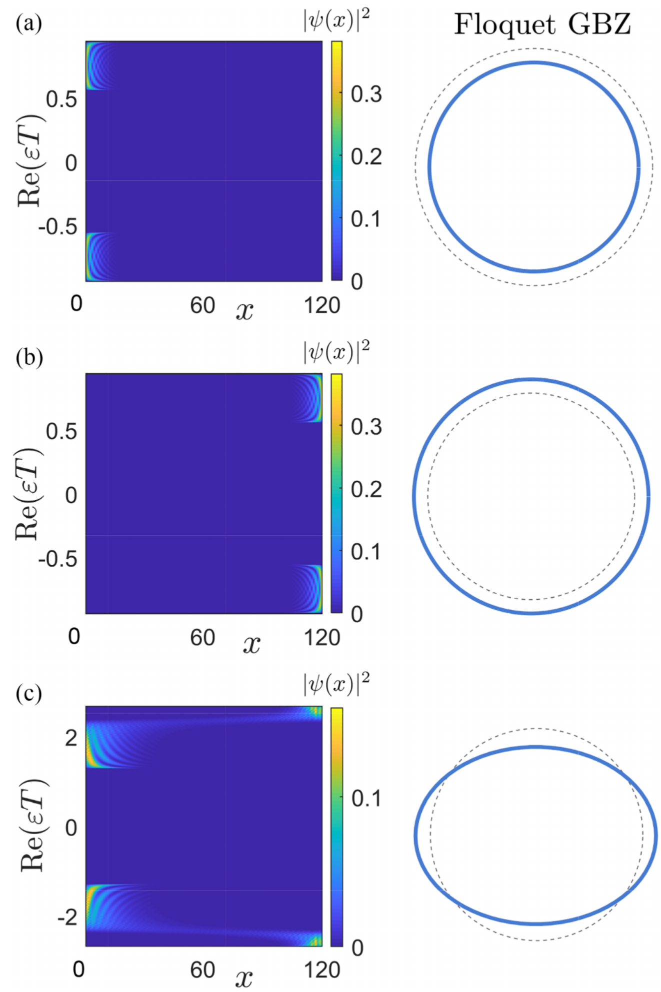

FIG. 6. Modulus square of all bulk eigenstates (left column) and schematic illustration of effective Floquet GBZs (right column) of Floquet systems with different parameters. In (a) and (b), the driving parameter is $t_2 = \pm 1$, and other parameters are set as $t_1 = 0.8$, $T_1{:}T_2 = 3{:}2$, $T = 0.3\pi$. The parameter γ is chosen as 0.1 for (a) and -0.1 for (b). The effective Floquet GBZs (blue solid) are circles with radius of $r_F = \sqrt{|\frac{t_1-\gamma}{t_1+\gamma}|}$. When the GBZ is within the unit circle as shown in (a), all bulk modes tend towards the left side. If the GBZ lies outside the unit circle as in (b), the bulk modes cumulate on the right. (c) Modulus square of eigenstates showing bipolar NHSE. The Floquet GBZ is an irregular closed curve that passes through the unit circle. The parameters of (c) are the same as in Fig. 4.

[Fig. 5(d)], thus, the traditional Bloch BBC still holds, despite the fact that the instantaneous Hamiltonian is nonreciprocal at any time.

IV. NON-HERMITIAN FLOQUET SKIN EFFECT

In addition to the appearance of anomalous Floquet topological phases, periodic driving can also bring some new features to NHSE. For the static non-Hermitian SSH model (1), all modes are accumulated at one edge of the system depending on the sign of non-Hermitian parameter γ. Hereafter, this phenomenon is referred as *unipolar* NHSE. For Floquet systems, such unipolar NHSE occurs when the Floquet GBZ

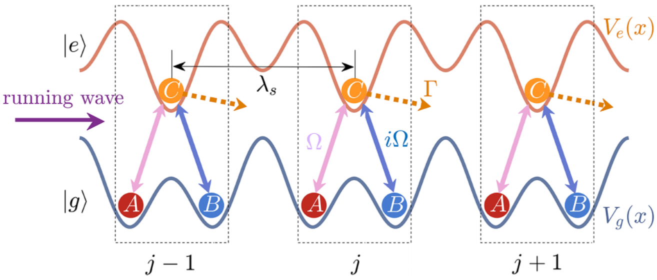

FIG. 7. Illustration of the scheme to implement the non-Hermitian SSH model. Atoms in two different states $|g\rangle$ and $|e\rangle$ feel different lattice potentials V_g and V_e with lattice constant λ_s. The motion of the state $|g\rangle$ in lattice potential V_g is dominated by a Hermitian SSH Hamiltonian. A running wave couples the stable state $|g\rangle$ and dissipative state $|e\rangle$ with dissipation rate Γ, resulting in an effective nonreciprocal hopping of $|g\rangle$ between sublattices A and B after adiabatic elimination.

does not intersect with the unit circle, i.e., lying completely inside or outside the unit circle, as shown in Figs. 6(a) and 6(b), where the driving parameter is t_2 and the Floquet GBZ is a circle with radius r_F as discussed in Sec. III A. In Fig. 6(a) [Fig. 6(b)], we find that all skin modes are located at the left (right) boundary of the one-dimensional chain when r_F is less (greater) than 1.

On the other hand, if GBZ of the effective Floquet Hamiltonian acquires an irregular shape with some part inside and some part outside the unit circle, such as the example of $f(t) = [t_2(t), \gamma(t)]$ discussed in Sec. III B, the skin modes are residing on both boundaries Fig. 6(c). This exotic feature, referred as *bipolar* NHSE, has been suggested and discussed in non-Hermitian systems with long-range hopping [54–56]. Here, with the aid of Floquet engineering, we show that NHSE can be realized in noninteracting systems with only nearest-neighbor hopping, which are less demanding in experiment. When transiting from the left-edge skin modes to the right-edge ones, there exist extended Bloch states connecting the two edges, which correspond to the intersection points of the Floquet GBZ and the unit circle. In the quasienergy spectrum, these points are the intersection of the OBC spectrum and the PBC spectrum, and are referred to as Bloch points [34].

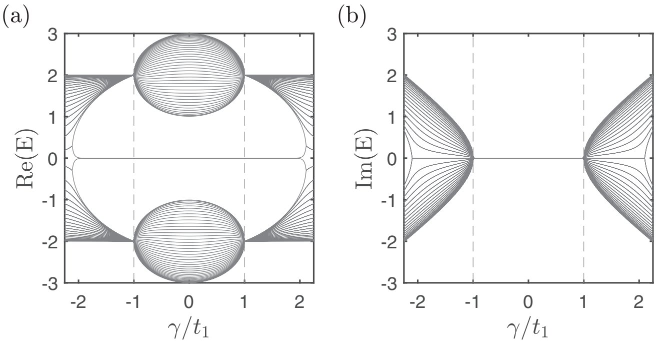

FIG. 8. (a) Real part and (b) imaginary part of the energy spectrum under OBC for the $\mathcal{PT}$ symmetry system of size $L = 40$, with varying γ/t_1 and fixed $t_2 = 2t_1$. The t_1 is chosen as the unit of energy.

The bipolar NHSE can also manifest the complex winding of the PBC spectrum. To study the winding of spectrum, we extend the definition used in Ref. [53] to two-band systems. For any given complex energy reference point $E_b \in \mathbb{C}$, the winding number of a two-band Bloch Hamiltonian $\mathcal{H}(k) = \boldsymbol{h}(k)\cdot\boldsymbol{\sigma}$ with $\boldsymbol{h} = (h_x, h_y, h_z)$ and $\boldsymbol{\sigma} = (\sigma_x, \sigma_y, \sigma_z)$ is defined as

$$W(E_b) = \frac{1}{2\pi}\oint_{1\mathrm{BZ}} \frac{d}{dk}\arg[\varepsilon_+^b(k) + \varepsilon_-^b(k)]dk, \tag{16}$$

where $\varepsilon_\pm^b = \varepsilon_\pm - E_b$ with the Bloch Hamiltonian eigenvalues $\varepsilon_\pm(k) = \pm\sqrt{\sum_{l=x,y,z} h_l^2(k)}$. The condition for the appearance of non-Hermitian skin modes is the existence of a $E_b \in \mathbb{C}$ to satisfy $W(E_b) \neq 0$. That is to say, as long as the energy spectrum of Bloch Hamiltonian forms a closed loop with a nonzero enclosed area, there exists non-Hermitian skin modes residing on one edge of the system determined by the loop winding.

Taking the example shown in Fig. 4(a), the Bloch points divide each band of the PBC spectrum into three loops in the complex quasienergy plane. The PBC spectrum surrounds the OBC spectrum except for Bloch points, so that for any quasienergy ε_O on the OBC spectrum that is not at Bloch points, there is a nontrivial winding $W(\varepsilon_O) \neq 0$. Hence, the eigenstate with quasienergy ε_O is a skin mode. The position of the skin mode depends on the sign of $W(\varepsilon_O)$, which is related to the winding of the loop surrounding ε_O. As illustrated in Fig. 4(a) and Fig. 6(c), the modes of OBC spectrum in clockwise loops correspond to the non-Hermitian skin modes distributed on the left end, and the ones in counterclockwise loops are distributed on the right end.

V. CONCLUSION AND EXPERIMENTAL IMPLEMENTATION

We investigate a non-Hermitian SSH model with nonreciprocal hopping parameters under periodic driving. The most fundamental impact of periodic driving on non-Hermitian topological systems is the change of the effective Floquet GBZ. On one hand, this would greatly increase the difficulty of calculating the effective Floquet GBZ, making it difficult to capture the topological characterization of non-Hermitian Floquet systems. Here we provide a method for calculating the Floquet GBZ without truncating the Hamiltonian, and demonstrate its ability under various typical driving schemes. On the other hand, the tunable Floquet GBZ provides us with a pathway to observe richer NHSEs, which may bring a new direction to the hybrid skin-topological effects. In particular, we find that bipolar NHSE, which usually requires long-range hopping [54,55] or intracell interaction [56] in static systems, can be realized in short-range models with the aid of proper Floquet driving. This finding not only enriches the understanding of Floquet engineering for non-Hermitian systems, but also suggests experimental proposals to realize the exotic bipolar NHSE, as the implementation of periodic driving is usually simpler than the fine tuning of long-range hopping and interaction.

As an example, next we show that the model discussed here can be implemented in cold atomic systems with a high degree of controllability. The Hermitian SSH model, $H_{\mathrm{SSH}} = \sum_j (t_1 a_j^\dagger b_j + t_2 a_{j+1}^\dagger b_j + \mathrm{H.c.})$, has be realized in cold atoms trapped in an optical lattice [90]. The non-Hermitian term, $\gamma a_j^\dagger b_j - \gamma b_j^\dagger a_j$, can be induced by coupling an unstable excited state that senses a different lattice potential [91]. Specifically, we consider a two-level system with stable state $|g\rangle$ and dissipative state $|e\rangle$ with loss rate Γ in a one-dimensional state-dependent optical lattice, as shown in Fig. 7. The lattice is formed by superimposing two standing waves $|\boldsymbol{E}_l(x)| = E_l \sin(k_l x)$ and $|\boldsymbol{E}_s(x)| = E_s \sin(k_s x + \pi/2)$, where E_l (E_s) are the amplitudes of the long-wavelength λ_l (short-wavelength $\lambda_s = \lambda_l/2$) lasers and $k_l = 2\pi/\lambda_l$ ($k_s = 2\pi/\lambda_s$). The optical potential felt by the stable (dissipative) states is

$$V_{g(e)}(x) = -(1/2)\alpha_{g(e)}(\lambda_s)E_s^2 \sin^2(k_s x + \pi/2) -(1/2)\alpha_{g(e)}(\lambda_l)E_l^2 \sin^2(k_l x), \tag{17}$$

where $\alpha_{s=g,e}(\lambda)$ denotes the polarizability of different atomic states, which is dependent on the wavelength of light and is generally different for different states. By choosing an appropriate wavelength and atomic states so that the atomic polarizabilities satisfy $\alpha_g(\lambda_{s/l}) < 0$ and $\alpha_e(\lambda_{s/l}) > 0$ [or $\alpha_g(\lambda_s) < 0$, $\alpha_g(\lambda_l) > 0$ and $\alpha_e(\lambda_{s/l}) > 0$], we obtain the state-dependent optical lattices shown in Fig. 7. In the tight-binding approximation, the behavior of the stable state $|g\rangle$ is governed by the Hermitian Hamiltonian $H_g = H_{\mathrm{SSH}}$ [90], while the non-Hermitian Hamiltonian for dissipative state $|e\rangle$ reads $H_e = \sum (t_e c_j^\dagger c_{j+1} + t_e c_{j+1}^\dagger c_j - i\Gamma c_j^\dagger c_j)$. Here the on-site operators are defined as $a_j^\dagger |0\rangle = |A, j\rangle$, $b_j^\dagger |0\rangle = |B, j\rangle$, and $c_j^\dagger |0\rangle = |C, j\rangle$, with $|C, j\rangle$ located in the middle of $|A, j\rangle$ and $|B, j\rangle$.

Then we apply a running wave with Rabi frequency Ω_r, parallel to the lattice, to couple the states $|C\rangle$ and $|A\rangle$ ($|B\rangle$). The coupling Hamiltonian is represented as $H_{ge} = (1/2)\sum_j [\Omega e^{ik_r j \lambda_s} c_j^\dagger (a_j + g_r b_j) + \mathrm{H.c.}]$, where k_r is the wave number of the running wave, $\Omega = \Omega_r \int dx e^{ik_r x} W_e(x) W_g(x - \lambda_s/4)$ with $W_{g,e}(x)$ being the Wannier function, and $g_r = \Omega_r \int dx e^{ik_r x} W_e(x) W_g(x + \lambda_s/4)/\Omega$. The single-photon detuning $\delta = \omega_r - \omega_{eg} - \Delta V$, where ω_r is the frequency of running-wave laser, ω_{eg} is the atomic frequency, and $\Delta V = V_e^{\min} - V_g^{\min}$ with potential energy minimum $V_g^{\min}$ ($V_e^{\min}$) of the stable (dissipative) lattice. When $\max\{\delta, \Gamma\} \gg \{\Omega, t_e, t_1, t_2\}$, we can adiabatically eliminate c_j to obtain an effective non-Hermitian Hamiltonian $H_{\mathrm{exper}} = H_{\mathrm{SSH}} - \frac{i}{2}\sum_j L_j^\dagger L_j$ [91], where $L_j = \kappa(a_j + g_r b_j)$ with $\kappa = \frac{\sqrt{\Gamma}|\Omega|}{\sqrt{\Gamma^2 + 4\delta^2}}$. By appropriately choosing the wave number of the running wave to ensure $g_r = i$, we can get

$$H_{\mathrm{exper}} = H_{\mathrm{SSH}} + \gamma \sum_j (a_j^\dagger b_j - b_j^\dagger a_j) - 2i\gamma N, \tag{18}$$

where $\gamma = \kappa^2/2$ and $2N = \sum (a_j^\dagger a_j + b_j^\dagger b_j)$. The last term $-2i\gamma N$ corresponds to a background loss. The ratio t_1/t_2 of hopping coefficients can be changed by adjusting the amplitudes of two standing wave lasers, and γ can be adjusted by changing the direction (reverse the laser), frequency, and amplitude of the running wave. Thus far, we present a scheme for implementing non-Hermitian SSH model (1) in cold atomic systems.

ACKNOWLEDGMENTS

This work is supported by the National Natural Science Foundation of China (Grants No. 12074428 and No. 92265208), and the National Key R&D Program of China (Grant No. 2022YFA1405301).

APPENDIX: THE HAMILTONIAN WITH $\mathcal{PT}$-SYMMETRY

Using the unitary matrix $U = (i\sigma_x + \mathbb{I}_2)/\sqrt{2} \otimes \mathbb{I}_L$, the non-Hermitian SSH model (1) can be transformed into a Hamiltonian $H_{\mathcal{PT}}$ with $\mathcal{PT}$ symmetry,

$$\begin{aligned} H_{\mathcal{PT}} = & \sum_j \left[t_1 (a_j^\dagger b_j + \mathrm{H.c.}) + i\gamma (a_j^\dagger a_j - b_j^\dagger b_j) \right] \\ & + \sum_j \left[\frac{it_2}{2} (a_{j+1}^\dagger a_j - b_{j+1}^\dagger b_j) \right. \\ & \left. + \frac{t_2}{2} (a_{j+1}^\dagger b_j + a_j^\dagger b_{j+1}) + \mathrm{H.c.} \right], \end{aligned} \tag{A1}$$

which satisfies $(\mathcal{PT})H(\mathcal{PT})^{-1} = H$ with the parity operator $\mathcal{P} = \sigma_x \otimes \mathbb{I}_L$, the time-reversal operator $\mathcal{T} = \mathcal{K} \otimes \mathbb{I}_L$, and the complex conjugate operator $\mathcal{K}$. The $\mathcal{PT}$ symmetry implies that the eigenvalues of $H_{\mathcal{PT}}$ can be all real [92], although the Hamiltonian is non-Hermitian. When the eigenstates preserve $\mathcal{PT}$ symmetry, the eigenvalues are real. When $\mathcal{PT}$ symmetry is broken, the eigenvalues exhibit nonzero imaginary parts. The transition point between the two cases is called the exceptional point (EP) [93], at which the eigenvalues degenerate and the corresponding eigenstates merge. Thus, the subspace dimension of degenerate eigenvalues collapses, and the Hamiltonian is defective. For the Hamiltonian (A1), the degeneracy condition of bulk bands is $|\gamma| = |t_1|$ [12], and the eigenvalues and their corresponding algebraic and geometric multiplicities [94] at this point can be accurately calculated.

We first consider the case of $\gamma = t_1$. Following the procedure given in Ref. [12], we calculate the characteristic polynomial $f(\lambda)$ of $H_{\mathcal{PT}}^2$ because $H_{\mathcal{PT}}^2$ is a block upper triangular matrix,

$$H_{\mathcal{PT}}^2 = \begin{pmatrix} t_2^2/2 & -it_2^2/2 & 2t_2\gamma & 0 & 0 & \cdots \\ it_2^2/2 & t_2^2/2 & 0 & 2t_2\gamma & 0 & \cdots \\ 0 & 0 & t_2^2 & 0 & 2t_2\gamma & \cdots \\ 0 & 0 & 0 & t_2^2 & 0 & \cdots \\ 0 & 0 & 0 & 0 & t_2^2 & \cdots \\ \vdots & \vdots & \vdots & \vdots & \vdots & \ddots \end{pmatrix}. \tag{A2}$$

It is easy to obtain that the characteristic polynomial of $H_{\mathcal{PT}}^2$ is $f(\lambda) = \lambda^2(\lambda - t_2^2)^{2L-2}$. Owing to the chiral symmetry of $H_{\mathcal{PT}}$, i.e., $\Gamma H_{\mathcal{PT}} \Gamma^{-1} = -H_{\mathcal{PT}}$ with $\Gamma = \sigma_y \bigotimes \mathbb{I}_L$, eigenvalues $(E, -E)$ always exist in pairs. Thus, the eigenvalues of Hamiltonian $H_{\mathcal{PT}}$ are $E = 0, t_2, -t_2$ with algebraic multiplicities $2, L-1, L-1$, respectively. By calculating the rank of

$(H_{\mathcal{PT}} - E)$, we can further obtain that the geometric multiplicities of the three eigenvalues are 1. This means that the two bulk bands undergo high degeneracy at $E = \pm t_2$, respectively, resulting in $(L-1)$-order EPs. At this point, the $\mathcal{PT}$-symmetry Hamiltonian $H_{\mathcal{PT}}$ is highly defective. For the case of $\gamma = -t_1$, $H_{\mathcal{PT}}^2$ is a block lower triangular matrix, and the eigenvalues of $H_{\mathcal{PT}}$, as well as the algebraic and geometric multiplicities of the eigenvalues, can be solved similarly, leading to consistent solutions as for $\gamma = t_1$.

In Fig. 8 we demonstrate the complex energy spectrum of $H_{\mathcal{PT}}$ under OBC. For $\gamma = 0$, $H_{\mathcal{PT}}$ is Hermitian, and all eigenvalues are obviously real. As $|\gamma/t_1|$ increases but stays below 1, the eigenvalues are all real, indicating that the $\mathcal{PT}$ symmetry is preserved. When $|\gamma/t_1| = 1$, the bulk bands degenerate at $E = \pm t_2$. As $|\gamma/t_1|$ further increases, degeneracy is lifted and nonzero imaginary parts appear in the energy spectrum, indicating that the $\mathcal{PT}$ symmetry is broken.

[1] Z. Lin, H. Ramezani, T. Eichelkraut, T. Kottos, H. Cao, and D. N. Christodoulides, Unidirectional invisibility induced by $\mathcal{PT}$-symmetric periodic structures, Phys. Rev. Lett. **106**, 213901 (2011).

[2] B. Peng, Ş. K. Özdemir, F. Lei, F. Monifi, M. Gianfreda, G. L. Long, S. Fan, F. Nori, C. M. Bender, and L. Yang, Parity-time-symmetric whispering-gallery microcavities, Nat. Phys. **10**, 394 (2014).

[3] A. Regensburger, C. Bersch, M.-A. Miri, G. Onishchukov, D. N. Christodoulides, and U. Peschel, Parity-time synthetic photonic lattices, Nature (London) **488**, 167 (2012).

[4] L. Ding, K. Shi, Q. Zhang, D. Shen, X. Zhang, and W. Zhang, Experimental determination of $\mathcal{PT}$-symmetric exceptional points in a single trapped ion, Phys. Rev. Lett. **126**, 083604 (2021).

[5] L. Ding, K. Shi, Y. Wang, Q. Zhang, C. Zhu, L. Zhang, J. Yi, S. Zhang, X. Zhang, and W. Zhang, Information retrieval and eigenstate coalescence in a non-Hermitian quantum system with anti-$\mathcal{PT}$ symmetry, Phys. Rev. A **105**, L010204 (2022).

[6] Y. Wu, W. Liu, J. Geng, X. Song, X. Ye, C.-K. Duan, X. Rong, and J. Du, Observation of parity-time symmetry breaking in a single-spin system, Science **364**, 878 (2019).

[7] H. Shen and L. Fu, Quantum Oscillation from in-gap states and a non-Hermitian Landau level problem, Phys. Rev. Lett. **121**, 026403 (2018).

[8] H. Zhou, C. Peng, Y. Yoon, C. W. Hsu, K. A. Nelson, L. Fu, J. D. Joannopoulos, M. Soljačić, and B. Zhen, Observation of bulk Fermi arc and polarization half charge from paired exceptional points, Science **359**, 1009 (2018).

[9] H. J. Carmichael, Quantum trajectory theory for cascaded open systems, Phys. Rev. Lett. **70**, 2273 (1993).

[10] S. Malzard, C. Poli, and H. Schomerus, Topologically protected defect states in open photonic systems with non-Hermitian charge-conjugation and parity-time symmetry, Phys. Rev. Lett. **115**, 200402 (2015).

[11] S. Diehl, E. Rico, M. A. Baranov, and P. Zoller, Topology by dissipation in atomic quantum wires, Nat. Phys. **7**, 971 (2011).

[12] T. E. Lee, Anomalous edge state in a non-Hermitian lattice, Phys. Rev. Lett. **116**, 133903 (2016).

[13] D. Leykam, K. Y. Bliokh, C. Huang, Y. D. Chong, and F. Nori, Edge modes, degeneracies, and topological numbers in non-Hermitian systems, Phys. Rev. Lett. **118**, 040401 (2017).

[14] F. K. Kunst, E. Edvardsson, J. C. Budich, and E. J. Bergholtz, Biorthogonal bulk-boundary correspondence in non-Hermitian systems, Phys. Rev. Lett. **121**, 026808 (2018).

[15] S. Yao and Z. Wang, Edge states and topological invariants of non-Hermitian systems, Phys. Rev. Lett. **121**, 086803 (2018).

[16] S. Yao, F. Song, and Z. Wang, Non-Hermitian Chern bands, Phys. Rev. Lett. **121**, 136802 (2018).

[17] H. Shen, B. Zhen, and L. Fu, Topological band theory for bon-Hermitian Hamiltonians, Phys. Rev. Lett. **120**, 146402 (2018).

[18] K. Yokomizo and S. Murakami, Non-Bloch band theory of non-Hermitian systems, Phys. Rev. Lett. **123**, 066404 (2019).

[19] D. S. Borgnia, A. J. Kruchkov, and R.-J. Slager, Non-Hermitian boundary modes and topology, Phys. Rev. Lett. **124**, 056802 (2020).

[20] N. Okuma, K. Kawabata, K. Shiozaki, and M. Sato, Topological origin of non-Hermitian skin effects, Phys. Rev. Lett. **124**, 086801 (2020).

[21] J. Y. Lee, J. Ahn, H. Zhou, and A. Vishwanath, Topological correspondence between Hermitian and non-Hermitian systems: Anomalous dynamics, Phys. Rev. Lett. **123**, 206404 (2019).

[22] T. Gao, G. Li, E. Estrecho, T. C. H. Liew, D. Comber-Todd, A. Nalitov, M. Steger, K. West, L. Pfeiffer, D. W. Snoke *et al.*, Chiral modes at exceptional points in exciton-polariton quantum fluids, Phys. Rev. Lett. **120**, 065301 (2018).

[23] J. Hou, Z. Li, X.-W. Luo, Q. Gu, and C. Zhang, Topological bands and triply degenerate points in non-Hermitian hyperbolic metamaterials, Phys. Rev. Lett. **124**, 073603 (2020).

[24] T. Liu, Y.-R. Zhang, Q. Ai, Z. Gong, K. Kawabata, M. Ueda, and F. Nori, Second-order topological phases in non-Hermitian systems, Phys. Rev. Lett. **122**, 076801 (2019).

[25] C. H. Lee, L. Li, and J. Gong, Hybrid higher-order skin-topological modes in nonreciprocal systems, Phys. Rev. Lett. **123**, 016805 (2019).

[26] J. M. Zeuner, M. C. Rechtsman, Y. Plotnik, Y. Lumer, S. Nolte, M. S. Rudner, M. Segev, and A. Szameit, Observation of a topological transition in the bulk of a non-Hermitian system, Phys. Rev. Lett. **115**, 040402 (2015).

[27] C. Poli, M. Bellec, U. Kuhl, F. Mortessagne, and H. Schomerus, Selective enhancement of topologically induced interface states in a dielectric resonator chain, Nat. Commun. **6**, 6710 (2015).

[28] X. Zhan, L. Xiao, Z. Bian, K. Wang, X. Qiu, B. C. Sanders, W. Yi, and P. Xue, Detecting topological invariants in nonunitary discrete-time quantum walks, Phys. Rev. Lett. **119**, 130501 (2017).

[29] L. Xiao, X. Zhan, Z. H. Bian, K. K. Wang, X. Zhang, X. P. Wang, J. Li, K. Mochizuki, D. Kim, N. Kawakami *et al.*, Observation of topological edge states in parity-time-symmetric quantum walks, Nat. Phys. **13**, 1117 (2017).

[30] S. Weimann, M. Kremer, Y. Plotnik, Y. Lumer, S. Nolte, K. G. Makris, M. Segev, M. C. Rechtsman, and A. Szameit, Topologically protected bound states in photonic parity-time-symmetric crystals, Nat. Mater. **16**, 433 (2017).

[31] A. Cerjan, S. Huang, M. Wang, K. P. Chen, Y. Chong, and M. C. Rechtsman, Experimental realization of a Weyl exceptional ring, Nat. Photonics **13**, 623 (2019).
[32] S. Weidemann, M. Kremer, T. Helbig, T. Hofmann, A. Stegmaier, M. Greiter, R. Thomale, and A. Szameit, Topological funneling of light, Science **368**, 311 (2020).
[33] F. Song, S. Yao, and Z. Wang, Non-Hermitian skin effect and chiral damping in open quantum systems, Phys. Rev. Lett. **123**, 170401 (2019).
[34] F. Song, S. Yao, and Z. Wang, Non-Hermitian topological invariants in real space, Phys. Rev. Lett. **123**, 246801 (2019).
[35] Y. Xiong, Why does bulk boundary correspondence fail in some non-Hermitian topological models, J. Phys. Commun. **2**, 035043 (2018).
[36] K. Kawabata, S. Higashikawa, Z. Gong, Y. Ashida, and M. Ueda, Topological unification of time-reversal and particle-hole symmetries in non-Hermitian physics, Nat. Commun. **10**, 297 (2019).
[37] H. Zhou and J. Y. Lee, Periodic table for topological bands with non-Hermitian symmetries, Phys. Rev. B **99**, 235112 (2019).
[38] K. Kawabata, K. Shiozaki, M. Ueda, and M. Sato, Symmetry and topology in non-Hermitian physics, Phys. Rev. X **9**, 041015 (2019).
[39] Y. Xu, S.-T. Wang, and L.-M. Duan, Weyl exceptional rings in a three-dimensional dissipative cold atomic gas, Phys. Rev. Lett. **118**, 045701 (2017).
[40] K. Moors, A. A. Zyuzin, A. Y. Zyuzin, R. P. Tiwari, and T. L. Schmidt, Disorder-driven exceptional lines and Fermi ribbons in tilted nodal-line semimetals, Phys. Rev. B **99**, 041116(R) (2019).
[41] J. Carlström and E. J. Bergholtz, Exceptional links and twisted Fermi ribbons in non-Hermitian systems, Phys. Rev. A **98**, 042114 (2018).
[42] H. Zhou, J. Y. Lee, S. Liu, and B. Zhen, Exceptional surfaces in $\mathcal{PT}$-symmetric non-Hermitian photonic systems, Optica **6**, 190 (2019).
[43] N. Hatano and D. R. Nelson, Localization transitions in non-Hermitian quantum mechanics, Phys. Rev. Lett. **77**, 570 (1996).
[44] M. S. Rudner and L. S. Levitov, Topological transition in a non-Hermitian quantum walk, Phys. Rev. Lett. **102**, 065703 (2009).
[45] K. Kawabata, T. Bessho, and M. Sato, Classification of exceptional points and non-Hermitian topological semimetals, Phys. Rev. Lett. **123**, 066405 (2019).
[46] K. Y. Bliokh and F. Nori, Klein-Gordon representation of acoustic waves and topological origin of surface acoustic modes, Phys. Rev. Lett. **123**, 054301 (2019).
[47] X.-W. Luo and C. Zhang, Higher-order topological corner states induced by gain and loss, Phys. Rev. Lett. **123**, 073601 (2019).
[48] A. McDonald, T. Pereg-Barnea, and A. A. Clerk, Phase-dependent chiral transport and effective non-Hermitian dynamics in a bosonic Kitaev-Majorana chain, Phys. Rev. X **8**, 041031 (2018).
[49] T.-S. Deng and W. Yi, Non-Bloch topological invariants in a non-Hermitian domain wall system, Phys. Rev. B **100**, 035102 (2019).
[50] Z. Yang, K. Zhang, C. Fang, and J. Hu, Non-Hermitian bulk-boundary correspondence and auxiliary generalized Brillouin zone theory, Phys. Rev. Lett. **125**, 226402 (2020).
[51] C. H. Lee and R. Thomale, Anatomy of skin modes and topology in non-Hermitian systems, Phys. Rev. B **99**, 201103(R) (2019).
[52] V. M. Martinez Alvarez, J. E. Barrios Vargas, M. Berdakin, and L. E. F. Foa Torres, Topological states of non-Hermitian systems, Eur. Phys. J.: Spec. Top. **227**, 1295 (2018).
[53] K. Zhang, Z. Yang, and C. Fang, Correspondence between winding numbers and skin modes in non-Hermitian systems, Phys. Rev. Lett. **125**, 126402 (2020).
[54] L. Zhang, Y. Yang, Y. Ge, Y.-J. Guan, Q. Chen, Q. Yan, F. Chen, R. Xi, Y. Li, D. Jia *et al.*, Acoustic non-Hermitian skin effect from twisted winding topology, Nat. Commun. **12**, 6297 (2021).
[55] H. Xin, W. Song, S. Wu, Z. Lin, S. Zhu, and T. Li, Manipulating the non-Hermitian skin effect in optical ring resonators, Phys. Rev. B **107**, 165401 (2023).
[56] Y. Qin and L. Li, Occupation-dependent particle separation in one-dimensional non-Hermitian lattices, Phys. Rev. Lett. **132**, 096501 (2024).
[57] D. Zou, T. Chen, W. He, J. Bao, C. H. Lee, H. Sun, and X. Zhang, Observation of hybrid higher-order skin-topological effect in non-Hermitian topolectrical circuits, Nat. Commun. **12**, 7201 (2021).
[58] N. Goldman and J. Dalibard, Periodically driven quantum systems: Effective Hamiltonians and engineered gauge fields, Phys. Rev. X **4**, 031027 (2014).
[59] M. Bukov, L. D'Alessio, and A. Polkovnikov, Universal high-frequency behavior of periodically driven systems: From dynamical stabilization to Floquet engineering, Adv. Phys. **64**, 139 (2015).
[60] A. Eckardt, Colloquium: Atomic quantum gases in periodically driven optical lattices, Rev. Mod. Phys. **89**, 011004 (2017).
[61] T. Kitagawa, E. Berg, M. Rudner, and E. Demler, Topological characterization of periodically driven quantum systems, Phys. Rev. B **82**, 235114 (2010).
[62] N. H. Lindner, G. Refael, and V. Galitski, Floquet topological insulator in semiconductor quantum wells, Nat. Phys. **7**, 490 (2011).
[63] W. Hu, J. C. Pillay, K. Wu, M. Pasek, P. P. Shum, and Y. D. Chong, Measurement of a topological edge invariant in a microwave network, Phys. Rev. X **5**, 011012 (2015).
[64] S. Mukherjee, A. Spracklen, M. Valiente, E. Andersson, P. Öhberg, N. Goldman, and R. R. Thomson, Experimental observation of anomalous topological edge modes in a slowly driven photonic lattice, Nat. Commun. **8**, 13918 (2017).
[65] L. J. Maczewsky, J. M. Zeuner, S. Nolte, and A. Szameit, Observation of photonic anomalous Floquet topological insulators, Nat. Commun. **8**, 13756 (2017).
[66] K.-Y. Shi, R.-Q. Chen, S. Zhang, and W. Zhang, Topological invariants of Floquet topological phases under periodical driving, Phys. Rev. A **106**, 053301 (2022).
[67] K. Shi, X. Zhang, and W. Zhang, Floquet topological phases with large winding number, Phys. Rev. A **109**, 013324 (2024).
[68] J. K. Asbóth, B. Tarasinski, and P. Delplace, Chiral symmetry and bulk-boundary correspondence in periodically driven one-dimensional systems, Phys. Rev. B **90**, 125143 (2014).
[69] T.-S. Xiong, J. Gong, and J.-H. An, Towards large-Chern-number topological phases by periodic quenching, Phys. Rev. B **93**, 184306 (2016).

[70] L. Jiang, T. Kitagawa, J. Alicea, A. R. Akhmerov, D. Pekker, G. Refael, J. I. Cirac, E. Demler, M. D. Lukin, and P. Zoller, Majorana fermions in equilibrium and in driven cold-atom quantum wires, Phys. Rev. Lett. **106**, 220402 (2011).

[71] L. Li, C. H. Lee, and J. Gong, Realistic Floquet semimetal with exotic topological linkages between arbitrarily many nodal loops, Phys. Rev. Lett. **121**, 036401 (2018).

[72] D. Carpentier, P. Delplace, M. Fruchart, and K. Gawedzki, Topological index for periodically driven time-reversal invariant 2D systems, Phys. Rev. Lett. **114**, 106806 (2015).

[73] X.-L. Qi, Y.-S. Wu, and S.-C. Zhang, General theorem relating the bulk topological number to edge states in two-dimensional insulators, Phys. Rev. B **74**, 045125 (2006).

[74] M. S. Rudner, N. H. Lindner, E. Berg, and M. Levin, Anomalous edge states and the bulk-edge correspondence for periodically driven two-dimensional systems, Phys. Rev. X **3**, 031005 (2013).

[75] M. S. Rudner and N. H. Lindner, Band structure engineering and non-equilibrium dynamics in Floquet topological insulators, Nat. Rev. Phys. **2**, 229 (2020).

[76] K. Wintersperger, C. Braun, F. N. Ünal, A. Eckardt, M. D. Liberto, N. Goldman, I. Bloch, and M. Aidelsburger, Realization of an anomalous Floquet topological system with ultracold atoms, Nat. Phys. **16**, 1058 (2020).

[77] J.-Y. Zhang, C.-R. Yi, L. Zhang, R.-H. Jiao, K.-Y. Shi, H. Yuan, W. Zhang, X.-J. Liu, S. Chen, and J.-W. Pan, Tuning anomalous Floquet topological bands with ultracold atoms, Phys. Rev. Lett. **130**, 043201 (2023).

[78] B. Höckendorf, A. Alvermann, and H. Fehske, Non-Hermitian boundary state engineering in anomalous Floquet topological insulators, Phys. Rev. Lett. **123**, 190403 (2019).

[79] M. Li, X. Ni,M. Weiner, A. Alù, and A. B. Khanikaev, Topological phases and nonreciprocal edge states in non-Hermitian Floquet insulators, Phys. Rev. B **100**, 045423 (2019).

[80] L. Zhou and J. Gong, Non-Hermitian Floquet topological phases with arbitrarily many real-quasienergy edge states, Phys. Rev. B **98**, 205417 (2018).

[81] L. Zhou, Non-Hermitian Floquet topological superconductors with multiple Majorana edge modes, Phys. Rev. B **101**, 014306 (2020).

[82] X. Zhang and J. Gong, Non-Hermitian Floquet topological phases: Exceptional points, coalescent edge modes, and the skin effect, Phys. Rev. B **101**, 045415 (2020).

[83] Y. Cao, Y. Li, and X. Yang, Non-Hermitian bulk-boundary correspondence in a periodically driven system, Phys. Rev. B **103**, 075126 (2021).

[84] H. Wu and J.-H. An, Floquet topological phases of non-Hermitian systems, Phys. Rev. B **102**, 041119(R) (2020).

[85] L. Jin and Z. Song, Bulk-boundary correspondence in a non-Hermitian system in one dimension with chiral inversion symmetry, Phys. Rev. B **99**, 081103(R) (2019).

[86] D.-W. Zhang, L.-Z. Tang, L.-J. Lang, H. Yan, and S.-L. Zhu, Non-Hermitian topological Anderson insulators, Sci. China Phys. Mech. Astron. **63**, 267062 (2020).

[87] A. Altland and M. R. Zirnbauer, Nonstandard symmetry classes in mesoscopic normal-superconducting hybrid structures, Phys. Rev. B **55**, 1142 (1997).

[88] X.-J. Liu, Z.-X. Liu, and M. Cheng, Manipulating topological edge spins in a one-dimensional optical lattice, Phys. Rev. Lett. **110**, 076401 (2013).

[89] C.-K. Chiu, J. C. Y. Teo, A. P. Schnyder, and S. Ryu, Classification of topological quantum matter with symmetries, Rev. Mod. Phys. **88**, 035005 (2016).

[90] M. Atala, M. Aidelsburger, J. T. Barreiro, D. Abanin, T. Kitagawa, E. Demler, and I. Bloch, Direct measurement of the Zak phase in topological Bloch bands, Nat. Phys. **9**, 795 (2013).

[91] Z. Gong, Y. Ashida, K. Kawabata, K. Takasan, S. Higashikawa, and M. Ueda, Topological phases of non-Hermitian systems, Phys. Rev. X **8**, 031079 (2018).

[92] C. M. Bender and S. Boettcher, Real spectra in non-Hermitian Hamiltonians having $\mathcal{PT}$ symmetry, Phys. Rev. Lett. **80**, 5243 (1998).

[93] W. D. Heiss, Exceptional points of non-Hermitian operators, J. Phys. A: Math. Gen. **37**, 2455 (2004).

[94] G. Golub and C. F. van Loan, *Matrix Computations* (Johns Hopkins University Press, Baltimore, 1996).